Structure of Organic Aerogels. 1. Morphology and Scaling

R. W. Pekala† and D. W. Schaefer*,‡

Chemistry & Materials Science Department, Lawrence Livermore National Laboratory, Livermore, California 94550, and Materials Research for Energy and Environmental Technology Department, Sandia National Laboratories, Albuquerque, New Mexico 87185-5800

Received April 5, 1993; Revised Manuscript Received July 19, 1993®

ABSTRACT: Small-angle X-ray scattering is used to determine the structure of nanoporous organic aerogels made by the base-catalyzed polymerization of resorcinol and formaldehyde. This study probes the effect of several variables on the morphology of the supercritically dried aerogels including catalyst concentration, monomer concentration, acid aging, and pyrolysis. In addition, the development of structure during polymerization and aging of the precursor aquagels is reported. The data are consistent with a smooth-surfaced morphology with no indication of fractal clusters or rough surfaces in the length-scale regime from 10 to 600 Å. These results, taken together, indicate that microphase separation is the dominant process underlying the morphology of these unique materials.

Introduction

Recently, Pekala *et al.*[1,2] demonstrated that certain organic reactions that proceed through sol–gel transitions can be used to form nanoporous aerogels. This new chemistry has largely involved the base-catalyzed, aqueous polymerization of resorcinol (1,3-dihydroxybenzene) with formaldehyde. The resultant aerogels have high porosities (>80%), high surface areas (400–900 m^2/g), ultrafine cell/pore sizes (<500 Å), and densities as low as 0.03 g/cm^3. Scanning and transmission electron microscopy (TEM) reveals (Figure 1) that the resorcinol–formaldehyde (RF) microstructure is composed of interconnected particle-like structures with diameters ranging from 30 to 200 Å. This microstructure is retained after pyrolysis at 1050 °C, resulting in the formation of vitreous carbon aerogels.[3]

Previous work has shown that polymerization conditions—viz., [resorcinol]/[catalyst] or R/C ratio—affect the structure and properties of these organic aerogels. In particular, the Brunauer–Emmett–Teller (BET) surface area increases monotonically with increasing catalyst (i.e., decreasing R/C). This increased surface area is the signature of decreasing the size scale of the backbone, consistent with electron microscopic observation.

The purpose of this paper is to investigate the relationship between preparative conditions and porosity using small-angle X-ray scattering (SAXS). Because the observed "particles" forming the network are on the order of 100 Å, the RF aerogels are ideally suited to analysis by SAXS. SAXS is sensitive to structural correlations in reciprocal space and yields the domain size, surface characteristics, and qualitative morphological features in the nanometer regime. In addition, surface areas, skeletal densities, and size scales of both the backbone and pores can be extracted from absolute intensity measurements.[4] Parameters associated with the samples studied are shown in Table I.

We investigate the consequences of several variables during the solution polymerization part of the synthesis including catalyst and monomer concentration. We also study the effect of acid aging following gelation. Finally, we compare the structure after pyrolysis of the supercritically dried aerogels. Although the scale of the structure is affected by all of the above parameters, we observe no qualitative deviation from smooth-surfaced two-phase morphology. Our results do indicate, however, that the colloidal aggregation model[5] for aerogel formation is *not* applicable to the RF system.

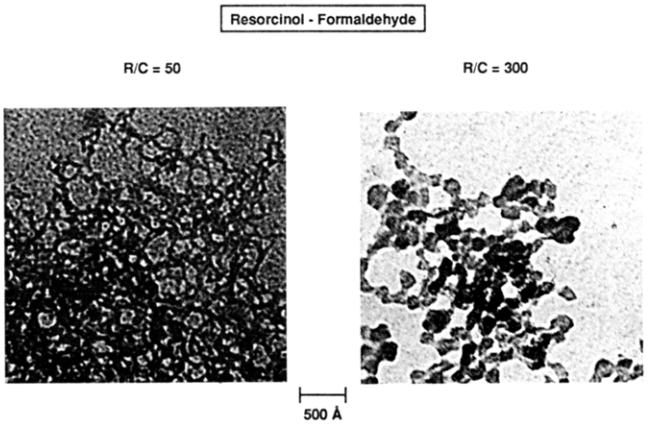

Figure 1. Transmission electron microscopic image of 5% RF aerogels at the extremes of catalyst concentration (R/C) studied.

Table I. Sample Parameters

sample name	R/C	R (% w/v)	density (g/cm^3)	BET SA (m^2/g)	Guinier radius (Å)	intercept (cm^{-1})
RF572	50	5	0.100	905	81.0	994
RF573	100	5	0.070	769	99.0	1100
RF590	150	5	0.061	699	107.0	1400
RF599	200	5	0.058	577	121.0	1930
RF648	300	5	0.065	389	148.0	4400
RF908	50	5	0.069		116.0	879
RF909	200	5	0.064		122.0	1691
RF910	300	5	0.061		155.0	4128
RF365	200	2	0.036		159.0	2280
RF394	200	3	0.042	534	151.0	2200
RF620	300	3	0.043		168.0	4927
RF796	50	15	0.207		40.0	778
RF479	200	15	0.152	556	80.0	2840
RF650	300	15	0.148		108.0	6290
CRF303	50	5	0.207	818	57.0	694
CRF598	100	5	0.136	764	78.0	1030
CRF313	150	5	0.099	709	95.0	1300
CRF611	200	5	0.103	683	94.0	1240
CRF448	300	5	0.085	586	150.0	5060
CRF327	50	4	0.197		72.0	1227
CRF568	200	3	0.067		135.0	2573
CRF612	300	3	0.065		152.0	4493

† Lawrence Livermore National Laboratory.
‡ Sandia National Laboratories.
● Abstract published in *Advance ACS Abstracts,* September 1, 1993.

0024-9297/93/2226-5487$04.00/0

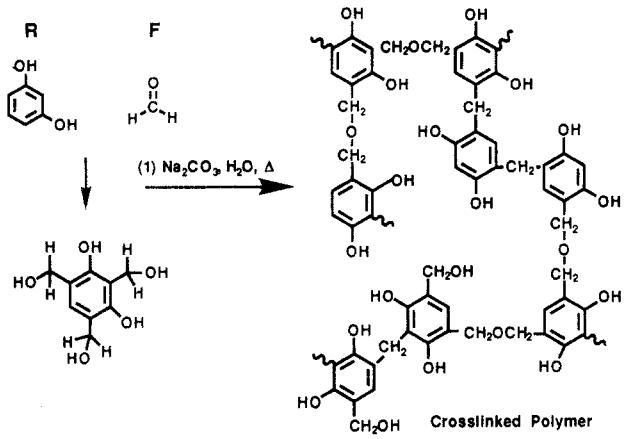

Figure 2. Schematic diagram of the polymerization process for the resorcinol–formaldehyde system.

The RF system contrasts with silica aerogels where kinetic growth processes lead to substantial structural diversity on the 100-Å length scale. Indeed, both "polymeric" and "colloidal" microstructures are realized depending on growth conditions in the solution precursors.[6-8] Many of these systems display self-similar or fractal morphology.

Fractal microstructures have not been observed for organic aerogels. Rather, smooth-surfaced domains seem universal for these materials, indicating that the synthetic opportunity afforded by kinetic growth processes is yet to be demonstrated. It appears that the dominant processes that determine structure in organic aerogels develop near equilibrium, accounting for the smooth-surfaced domains (at least on scales exceeding 10 Å, the lower limit of our measurements) correlated in a non-self-similar fashion. We present experimental data on precursor solution growth that implicates microphase separation, induced and limited by cross-linking as the dominant process leading to the observed morphology.

Background

The structure and properties of organic aerogels depends upon the amount of catalyst used in the aqueous, sol–gel polymerization.[1] The RF polymerization is conducted under alkaline conditions using sodium carbonate as the base catalyst. Because the pH of the RF solution decreases as the polymerization proceeds, each formulation is referenced by the [resorcinol]/[catalyst] or R/C ratio in the mixture. R/C ratios of 50–300 provide an acceptable range in which transparent gels and aerogels can be formed.

In the sol–gel polymerization, resorcinol serves as a trifunctional monomer capable of reaction at the 2-, 4- and/or 6-ring positions. Resorcinol reacts with formaldehyde under alkaline conditions to form mixtures of addition and condensation products. These intermediates further react to form a cross-linked polymer network. The two major reactions include (1) the formation of hydroxymethyl ($-CH_2OH$) derivatives of resorcinol and (2) the condensation of the hydroxymethyl derivatives to form methylene ($-CH_2-$) and methylene ether ($-CH_2OCH_2-$) bridged compounds.[9-11] Figure 2 shows a schematic diagram of the resorcinol–formaldehyde reaction.

The R/C ratio affects the density, BET surface area, and mechanical properties of the dried aerogels.[1,2,12-14] In previous experiments, RF gels were synthesized at 5% w/v reactants with different R/C ratios. If shrinkage did not occur during supercritical extraction, a final density of 0.05 g/cm^3 would have been expected. The greatest amount of shrinkage occurs for gels prepared under high catalyst conditions (i.e., low R/C ratios). The relationship between the final aerogel density and the R/C ratio is not linear. In fact, final densities plateau at a value ~15% higher than the target value for $R/C \geq 150$.

The effect of the R/C ratio upon density also manifests itself during the pyrolysis to carbon. In all cases, a 50% mass loss is experienced upon pyrolysis at 1050 °C, but the amount of volumetric shrinkage and the accompanying densification are linked to the R/C ratio in the original formulation. For RF aerogels prepared at 5% w/v reactants under high catalyst conditions (i.e., $R/C = 50$), the density increases ~100% in going from the cross-linked polymer to pure carbon. At the other extreme of our catalyst conditions (i.e., $R/C = 300$), the density increases ~40% in going from the cross-linked polymer to pure carbon.

The BET surface area, as determined by nitrogen adsorption, and the compressive moduli of organic aerogels show an inverse relationship with the R/C ratio. In general, aerogels with high surface areas and high compressive moduli are produced at $R/C = 50$. In contrast, aerogels with low surface areas and low compressive moduli are produced at $R/C = 300$. Carbon aerogels are an order of magnitude stiffer than their RF counterparts when compared at equivalent densities and R/C ratios.

The effects of the R/C ratio upon the density, surface area, and mechanical properties of organic aerogels suggest differences in their microstructure. Figure 1 shows TEMs of RF aerogels prepared at the extremes of our catalyst conditions. Each aerogel is composed of interconnected particles, giving a "string of pearls" appearance. At $R/C = 50$, the particles have diameters of ~30 Å and are tightly fused together, imparting a fibrous network appearance. At $R/C = 300$, the particles have diameters of ~200 Å and appear to be loosely bonded.

Experimental Section

The preparation of RF gels and aerogels has been described previously.[1] A typical formulation contained 0.29 M resorcinol, 0.57 M formaldehyde, and 1–6 mM sodium carbonate for a total of 5% w/v reactants. RF solutions were poured into glass vials, sealed, and cured for 7 days at 85–95 °C. Upon removal from their containers, the gels were placed in a dilute acid solution at 40–50 °C to maximize cross-link density through further condensation of hydroxymethyl ($-CH_2OH$) groups. Aerogels prepared by this process are designated as "RF".

To access the effect of the acid wash, a family of aerogels was also prepared without the acid wash. These unwashed (URF) gels were otherwise dried exactly as the acid-washed (RF) materials.

Both the RF and URF aquagels were solvent exchanged with acetone to achieve compatibility with CO_2. The solvent-filled gels were placed in a jacketed pressure vessel (Polaron, Watford, England) and covered with liquid CO_2. After sufficient exchanges with CO_2 to remove the organic solvent, the vessel was taken above the critical point ($T_c = 31$ °C; $P_c = 7.4$ MPa). The resultant RF aerogels were dark red but still transmitted light.

Carbon aerogels (CRF) were formed from the pyrolysis of RF aerogels in a Lindberg three-zone furnace. The furnace was evacuated and backfilled with nitrogen after the samples were loaded. Nitrogen (<1 ppm oxygen) flowed through the furnace at 2 L/min during the pyrolysis cycle. The furnace was heated at ~1.5 °C/min to 1050 °C and held at this temperature for 4 h. The furnace was then cooled to room temperature under its own thermal mass.

Aerogel densities were determined by weighing and measuring the samples after desiccation for a minimum of 24 h. Thin slices (1–2 mm) were precision machined from the aerogels for all scattering experiments. Samples were packaged in aluminum holders with Mylar tape windows.

Small-angle X-ray scattering was performed under the 10-m point-collimated instrument at the Oak Ridge National Labo-

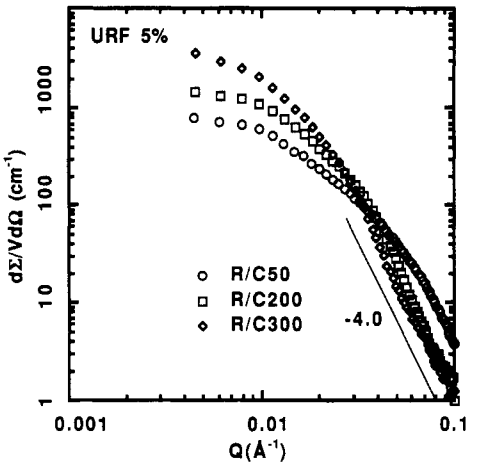

Figure 3. SAXS data for URF aerogels synthesized at the monomer concentration (5% w/v) but different R/C ratios. R = resorcinol molar concentration, C = catalyst molar concentration. URF aerogels were not subject to acid aging following gelation.

ratory. Cu Kα incident radiation was derived from a rotating-anode generator operating at approximately 300 W. All scattering angles were collected simultaneously using a 2-dimensional position-sensitive detector with a resolution of approximately 1 mm. The sample detector distance was 5 m. Approximately 10^6 counts were collected for each sample, taking typically 10 min. The data were corrected for detector sensitivity and dark current. A negligible background derived from an empty sample holder was subtracted.

The total scattering cross section per unit volume Σ/V was calculated from the measured differential scattering cross sections $d\Sigma/V\,d\Omega$. Σ/V was less than 0.05 cm^{-1} for all samples studied, indicating that less than 1% of the incident beam is scattered by a 2-mm sample. Measured sample transmission coefficients were typically 0.8.

We were alert to the possible presence of fractal networks in our aerogels. Disordered materials such as aerogels often display dilation symmetry,[5,8] and small-angle scattering is a convenient method for determining the fractal dimensions (D_m, D_s). For fractal structures, the SAXS intensity $I(Q)$ shows a power law dependence on the magnitude of the scattering vector, Q, such that

mass fractal:

$$I(Q) \sim Q^{-D_m} \qquad 1 < D_m < 3 \tag{1}$$

surface fractal:

$$I(Q) \sim Q^{-(6-D_s)} \qquad 3 < 6 - D_s < 4 \tag{2}$$

D_m describes the geometry of self-similar network structures and varies from 1 for a nonlinear rodlike configuration to 3 for a uniformly dense structure. D_s, on the other hand, describes surface roughness and varies between 2 and 3, the former being the dimension of a smooth surface and the latter being the limit where roughness becomes uniform porosity. For smooth surfaces the limiting Porod slope is $-(6 - D_s) = -4.0$.

Our results show no mass-fractal power-law regime for any of the materials studied. That is, all observed power-law profiles have limiting high-Q exponents equal to −4.0. Although it is possible that fractal behavior, similar to that observed for silica aerogels,[5,15] might be found if samples of sufficiently low density could be made, it appears to us that the self-similar kinetic growth processes are not dominant for organics. Indeed, the observation of smooth surfaces suggests that near-equilibrium processes are controlling structural development.[16]

Results: Aerogels

Figures 3–5 show log–log plots of SAXS intensity in absolute units (differential scattering cross section per unit sample volume, $d\Sigma/V\,d\Omega$) versus scattering vector, Q,

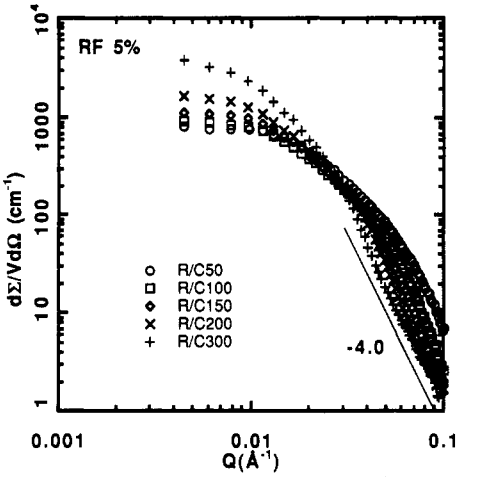

Figure 4. SAXS data for the acid-aged RF aerogel. Acid aging strengthens the gel, leading to less collapse on supercritical drying.

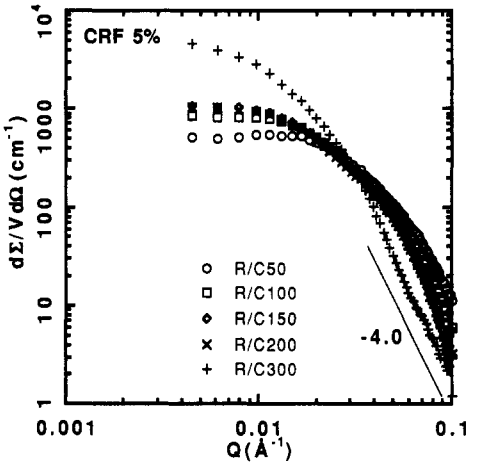

Figure 5. SAXS data for CRF carbonized aerogel synthesized at 5% monomer concentration.

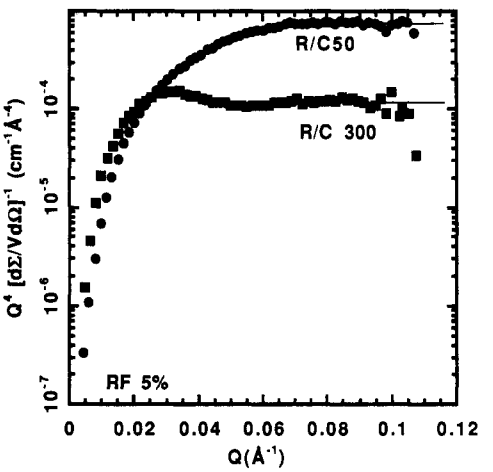

Figure 6. Porod plot for the 5% RF aerogels at R/C = 50 and 300.

for URF, RF, and CRF aerogels synthesized at various R/C ratios. For each curve, a constant intensity is observed at small values of Q, consistent with a unform long-range structure—i.e., the aerogels are homogeneous at length scales >500 Å. In addition, a limiting slope of −4.0 is found for all the materials, as revealed more clearly in Figure 6 which shows a Porod plot ($Q^4\,d\Sigma/V\,d\Omega$ vs Q) for the extremes of R/C. This plot shows variability in structure at intermediate length scales but universal limiting behavior consistent with smooth surfaces.

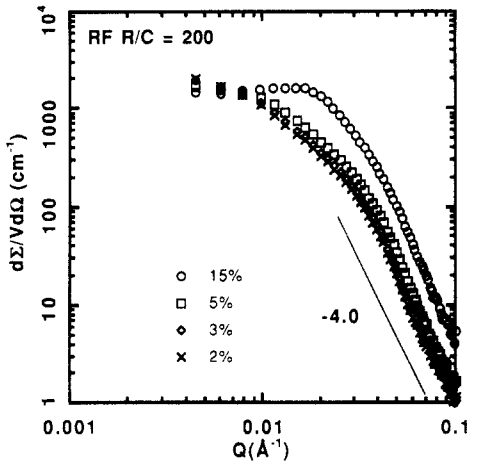

Figure 7. Concentration dependence of RF scattering profiles at $R/C = 200$. A peak emerges at high monomer concentration.

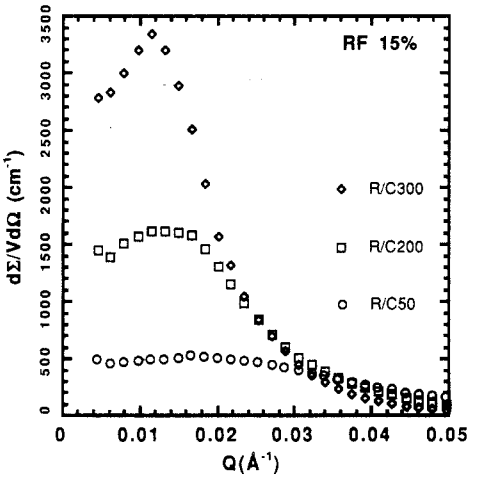

Figure 8. SAXS data on a linear scale showing an R/C-dependent peak for RF aerogels synthesized at the same monomer concentration (15% w/v).

More generally, the data reveal monotonic trends with the R/C ratio, although a peak develops at low R/C for the RF and CRF aerogels. The peak is more distinct for higher density materials as shown in Figure 7 which shows the concentration dependence of the scattering curves for RF materials synthesized at $R/C = 200$. At the highest concentration ($R = 15\%$), the peak is observed at all R/C ratios for all three classes of materials. The progression with catalyst concentration is displayed in Figure 8 on a linear scale showing a monotonic shift of the peak to smaller Q with decreasing catalyst.

The effect of acid washing and pyrolysis is shown in Figures 9 and 10 which compare URF, RF, and CRF materials at 5% and $R/C = 50$ and 300. At $R/C = 300$ (Figure 10), acid aging and carbonization are seen to shift the curves on the abscissa, corresponding to a simple change of length scale associated with the shrinkage of the sample but no qualitative change in the structure. At $R/C = 50$ (Figure 9), on the other hand, the shape of the curves changes with both washing and pyrolysis corresponding to structural rearrangement.

The appearance of the peak in the scattering profile only after carbonization of the high catalyst aerogels (Figure 9) is quite interesting and indicates that there are some latent correlations in the RF aerogel that are amplified by carbonization. These observations probably hold the key to identification of the growth process responsible for the structure (see below).

The similarity of the curves in Figure 10 suggests that much of the data might be superimposed by scaling of the

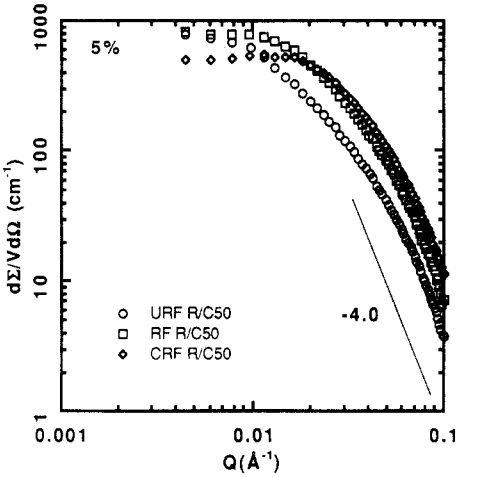

Figure 9. Scattering data showing the development of a peak on carbonization of the high catalyst RF aerogels. Substantial changes in structure occur on aging (URF to RF) and carbonization (RF to CRF).

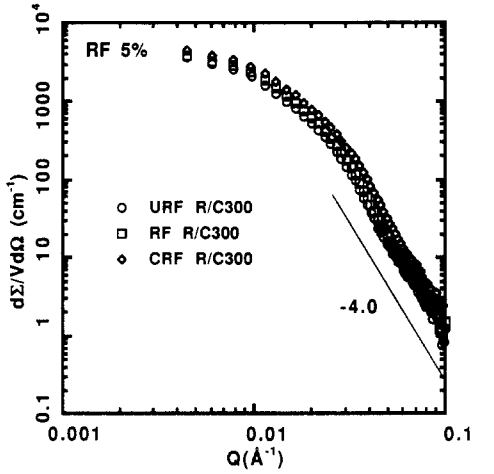

Figure 10. Scattering data for aerogels synthesized at $R/C = 300$ as a function of treatment. Apart from changes in the absolute intensity, little change is observed with either aging or carbonization, implying a simple length-scale-independent scaling of the pore structure.

abscissa and ordinate. The appropriate scaling variables are extracted from the intercept and initial curvature of the data using Guinier analysis,

$$I(Q) = d\Sigma/V\,d\Omega \sim I(0)[1 - (1/3)R_G^2Q^2 + ...] \quad (3)$$

The measured Guinier radius, R_G, and intercept, $I(0)$, are listed in Table I. Figure 11 shows the dependence of R_G on R/C for the three classes of materials. For those data where a peak is found, the measured Guinier radius is taken from the curvature on the high-Q shoulder of the peak. This procedure lacks theoretical justification but provides at least a qualitative measure of the length scale associated with the system. At low density, R_G is a measure of the smallest length scale in the system (~solid chord) which can then be used to scale the data leading to Figures 12–14. Figure 13 shows that the carbonized aerogels at 5% show similar scaling. The RF materials (Figure 12), on the other hand, deviate substantially from scaling behavior above $R/C = 150$. For both the RF and CRF materials, the deviations from scaling behavior become substantial at higher densities as shown in Figure 14.

The deviations from scaling behavior in Figure 12 imply at least two length scales are required to describe the structure of the RF aerogels between 10 and 500 Å. The largest length scale is the correlation range or Guinier

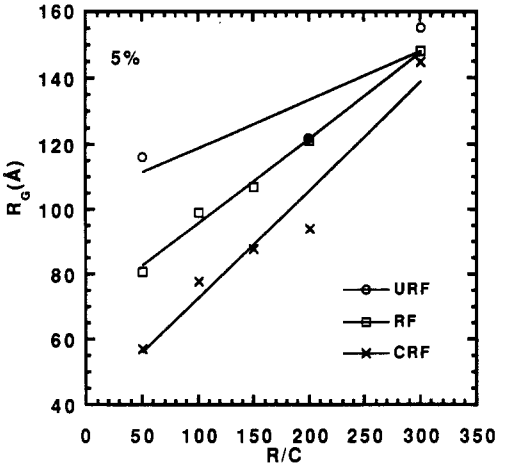

Figure 11. Dependence of the Guinier radius for RF, URF, and CRF aerogels on the R/C ratio. The large change in R_G at high catalyst (low R/C) implies substantial collapse of the structure on both aging and carbonization. R_G is porportional to the solid chord at low volume fraction.

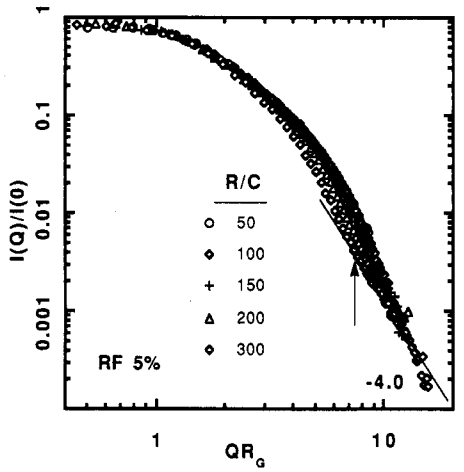

Figure 12. Scaled RF scattering data at 5% monomer concentration. At least two length scales are required to describe the structure, the correlation range ξ and a length below which the interface is simply a smooth surface. The lack of superposition at intermediate Q implies that the two lengths do not scale in a similar fashion at each R/C ratio. We trace this second length scale to a transition from nucleation-and-growth to spinodal decomposition during the polymerization.

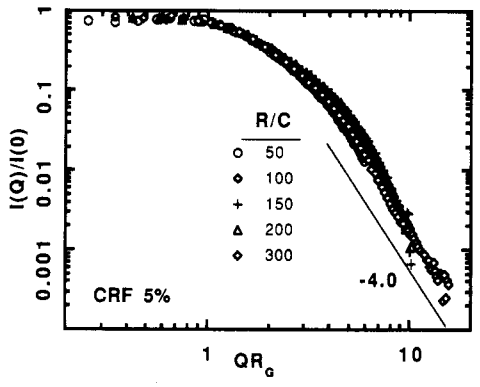

Figure 13. Scaled scattering data for carbonized aerogels. Near-superposition of the curves implies that after carbonization the pair of length scales needed to describe the structure scales with density in a similar fashion.

radius used to scale the data. A second length scale, however, appears that represents the length below which the structure is simply a smooth surface. This length scale is indicated by the vertical arrow in Figure 12 for R/C = 300 and is seen to move to larger QR_G with increasing

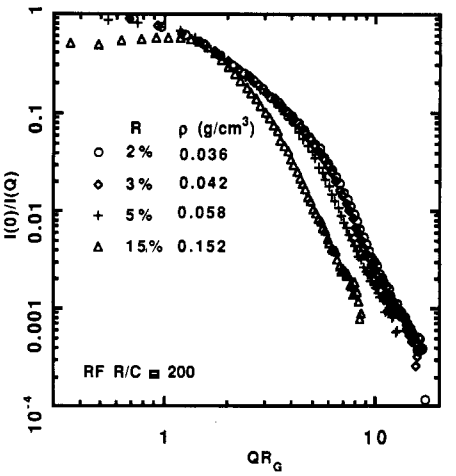

Figure 14. Scaled SAXS data as a function of density of the final RF aerogel. Lack of scaling implies a change in the underlying growth process as a function of density which is in turn determined by the initial concentration.

catalyst concentration. This progression implies that the two length scales are more widely separated at high catalyst compared to low.

Discussion

The persistent observation of peaks in the scattering curves, the absence of self-similar correlations, and the observation of short-scale smooth-surfaced morphology imply that the dominant process underlying structural development occurs near equilibrium.[16] Microphase separation, similar to that observed by Ulibarri *et al.*[17] for filled siloxanes, is the most reasonable process consistent with the data. That is, as polymerization proceeds, the increasing molecular weight and branching of the polymers reduce the entropy of mixing, thereby inducing phase separation. The cross-linked nature of the gel, however, precludes phase separation on large scales and restricts phase separation to domains whose scale is determined by the elastic modulus of the network.

Both de Gennes[18] and Bettachy *et al.*[19] show that the domain size in microphase-separated polymer/polymer blends is controlled by cross-link density, with larger domains expected for weakly branched systems because of the reduced modulus. The polymer/solvent system studied here should be qualitatively similar in that large-scale phase separation is precluded due to the energy cost of both stretching and compressing chains from their preferred configuration. Evidence based on the modulus and NMR show that the cross-link density of the aerogels increases with catalyst concentration, consistent with the observed decrease in domain size with catalyst.

Further insight into the mechanism of domain formation comes from observations of gel precursors. Figure 15 shows the measured SAXS profiles for solutions containing 5% w/v reactants at the extremes of the R/C ratio. Data taken at 2.5 h (not shown) are essentially identical to the 13-h data. These solutions were polymerized at 85 °C but removed temporarily and measured at room temperature. After the data of Figure 15 were taken the samples were stored at room temperature for 6 months and remeasured. In both cases, the peak was replaced by monotonic Guinier-like behavior.

In summary, the gel precursors show a strong peak in the scattering curve that changes little with polymerization time but it eventually disappears with aging. In addition, the peak position is consistent with smaller domains due to a higher cross-link density at high catalyst ratios. It is

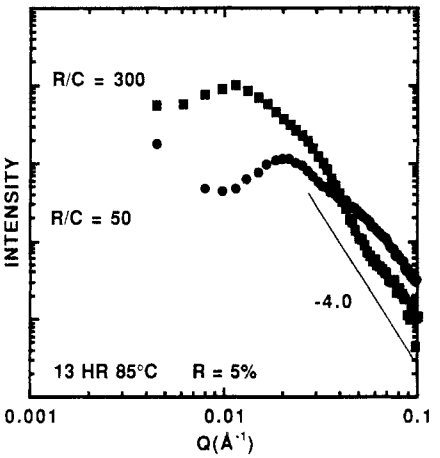

Figure 15. SAXS data for the sol precursors after 13 h at 85 °C. No change in the profile is observed between 2.5 and 13 h. After 6 months at room temperature, the peak in the scattering curve is not observed.

also interesting that the domains do not grow appreciably after 2.5 h, roughly the time where titration data show all resorcinol is consumed.

The microphase separation model implies that the domain size should vary strongly with catalyst concentration and weakly with overall density. In a forthcoming paper,[4] we further analyze the SAXS data on these aerogels and show that the mean solid chord of the string-of-pearls network does indeed vary monotonically with the R/C ratio but shows a much weaker dependence on the resorcinol concentration.

The emergence of a peak at both a high concentration and high R/C ratio probably reflects a transition from nucleation-and-growth to spinodal decomposition. As polymerization proceeds, we expect the incompatible region of the temperature–concentration phase diagram to expand, eventually leading to phase separation except at very high or low concentration. Near the critical isochore (the concentration at the maximum of the incompatible regime), phase separation occurs by spinodal decomposition, the signature of which is a peak in the scattering profile. At lower concentration, polymer droplets nucleate, leading to a particulate appearance and, at least in the early stages, no peak in the scattering profile. Since the phase diagram changes with cross-linking, transitions between the two classes of growth are possible. We believe such transitions occur as a function of both the concentration and the catalyst ratio density. These concepts will be explored further in the second paper in this series.

Since all of our samples are dilute in the polymer phase, a simple transition might be anticipated, with increasing concentration, from nucleation-and-growth to spinodal decomposition. Similarly, increased catalyst would yield denser cross-linking, effectively increasing the unfavorable interaction (χ parameter) between polymer and solvent fostering a similar transition. Throughout the variable space investigated, then, it is reasonable that a transition take place from nucleation-and-growth to spinodal decomposition as polymerization proceeds, explaining the string-of-pearls appearance (Figure 1).

The transition from nucleation-and-growth to spinodal decomposition accounts for the existence of two length scales observed in the scaled data. The larger length is the final domain size determined by competing entropic and enthalpic factors whereas the smaller is the domain size at the transition from the nucleation-and-growth to spinodal decomposition. In Figure 12, for example, the two lengths scales are closer in magnitude for the weakly branched $R/C = 300$ system compared to the more densely cross-linked $R/C = 50$ counterpart. Such a trend is expected since the more weakly branched system would persist longer in the nucleation regime leading to larger particles before becoming unstable to spinodal decomposition. The less particulate, more fused character of the string of pearls in the high catalyst systems is also consistent with an early transition to the spinodal regime at high catalyst.

Although our results do not preclude early-stage monomer–cluster growth proposed by LeMay *et al.*,[13] they do imply that the smooth-surfaced microstructure observed arises from phase separation, rather than kinetic growth via a monomer–cluster mechanism. Indeed, NMR, chromatography, and titration data all show that the resorcinol monomer is depleted rapidly, precluding sustainable monomer–cluster growth. It appears that, insofar as kinetic processes play any role at all, the essential process is cluster–cluster cross-linking, leading to incompatibility and microphase separation.

The single observation that seems inconsistent with the microphase separation model is the greater collapse of high catalyst materials on supercritical drying. Since the high-catalyst aerogels are demonstrably stiffer, one would expect greater resistance to collapse compared to the low-catalyst analogs. Apparently nonlinear effects control the collapse during solvent extraction.

Although the RF materials contrast with the widely accepted colloid aggregation model for base-catalyzed silica aerogels,[5,15] there is adequate evidence for near-equilbrium processes in silica aerogels as well.[20] For densities >0.1 g/cm^3 there is little evidence for either mass-fractal self-similarity characteristic of particle aggregation. Because of the lower skeletal density of RF compared to silica, one would expect particle growth and aggregation only at densities below 0.05 g/cm^3, near the lower limit of aerogel formation.

Summary

Organic aerogels are low-density, porous solids that have ultrafine cell/pore sizes and a solid matrix composed of interconnected colloidal-like particles with diameters of 30–200 Å. These materials are derived from the supercritical drying of cross-linked gels formed from the aqueous, sol–gel polymerization of resorcinol with formaldehyde. The structure and properties of both RF and carbon aerogels are largely determined by the catalyst concentration used in the polymerization. At high catalyst, dense cross-linking leads to microphase separation with small domains ($R_G \sim 80$ Å), whereas the degree of branching is reduced at low catalyst, leading to larger domains ($R_G \sim 150$ Å). In all cases, smooth-surfaced domains are found whose size decreases with increased cross-linking in the gel precursor.

The dominant process controlling the morphology is phase separation restricted to nanometer size scales by polymer cross-linking. This observation should strongly modify strategies to control the porosity of these materials.

Acknowledgment. This work was performed under the auspices of the U.S. Department of Energy by Lawrence Livermore National Laboratory under Contract No. W-7405-ENG-48 and by Sandia National Laboratories under Contract No. DE-AC04-76DP00789. We thank J. S. Lin and S. Spooner for their guidance in performing the SAXS experiments at Oak Ridge National Laboratory.

References and Notes

(1) Pekala, R. W. *J. Mater. Sci.* **1989**, *24*, 3221.
(2) Pekala, R. W.; Kong, F. M. *J. Phys. Colloq.* **1989**, *C4-33*, 50.

(3) Pekala, R. W.; Kong, F. M. *Polym. Prepr. (Am. Chem. Soc., Div. Polym. Chem.)* **1989**, *30*, 221.
(4) Part 2: Schaefer, D. W.; Pekala, R. W., to be published.
(5) Schaefer, D. W.; Keefer, K. D. *Phys. Rev. Lett.* **1986**, *56*, 2199–2202.
(6) Schaefer, D. W. *J. Phys., Colloq.* **1988**, *C4-24*, 121–126.
(7) Schaefer, D. W.; Brinker, C. J.; Wilcoxon, J. P.; Wu, D. Q.; Phillips, J. C.; Chu, B. In *Better Ceramics Through Chemistry III*; Brinker, C. J., Clark, D. E., Ulrich, D. R., Eds.; Materials Research Society: Pittsburgh, PA, 1988; Vol. 121; pp 691–696.
(8) Schaefer, D. W.; Wilcoxon, J. P.; Keefer, K. D.; Bunker, B. C.; Pearson, R. K.; Thomas, I. M.; Miller, D. E. In *Physics and Chemistry of Porous Media II*; Banavar, J. R., Koplik, J., Winkler, K. W., Eds.; American Institute of Physics: New York, 1987; Vol. 154; p 1.
(9) Werstler, D. D. *Polymer* **1986**, *27*, 757.
(10) Sebenik, A.; Osredkar, U.; Vizovisek, I. *Polymer* **1990**, *31*, 804.
(11) Pekala, R. W.; Ward, R. L. *Polym. Prepr. (Am. Chem. Soc., Div. Polym. Chem.)* **1990**, *31*, 167.
(12) Pekala, R. W.; Alviso, C. T.; LeMay, J. D. *J. Non-Cryst. Solids* **1990**, *125*, 67.
(13) LeMay, J. D.; Hopper, R. W.; Hrubesh, L. W.; Pekala, R. W. *MRS Bull.* **1990**, *15*, 19–45.
(14) LeMay, J. D.; Pekala, R. W.; Hrubesh, L. W. *Pac. Polym. Prepr.* **1989**, *1*, 295.
(15) Vacher, R.; Woignier, T.; Pelous, J.; Courtens, E. *Phys. Rev. B* **1988**, *37*, 6500.
(16) Schaefer, D. W.; Bunker, B. C.; Wilcoxon, J. P. *Proc. R. Soc. London A* **1989**, *A423*, 35.
(17) Ulibarri, T.; Beaucage, W. G.; Schaefer, D. W.; Assink, R. A.; Olivier, B. J. In *Polymer Based Microcomposites*; Baney, R. H., Gilliom, L. R., Hirano, S.-I., Schmidt, H. K., Eds.; Materials Research Society: Pittsburgh, PA, 1992; Vol. 274, pp 85–90.
(18) de Gennes, P.-G. *J. Phys. Lett.* **1979**, *40*, 69.
(19) Bettachy, A.; Derouiche, A.; Benhamou, M.; Daoud, M. *J. Phys., Lett.* **991**, 153–158.
(20) Schaefer, D. W.; Hurd, A. J. *Proc. Electrochem. Soc.* **1985**, *85*, 54.